JOURNAL OF GEOPHYSICAL RESEARCH, VOL. 113, C10005, doi:10.1029/2007JC004599, 2008

Modeling the impact of polar mesocyclones on ocean circulation

Alan Condron,[1] Grant R. Bigg,[2] and Ian A. Renfrew[3]

Received 19 October 2007; revised 12 May 2008; accepted 2 June 2008; published 10 October 2008.

[1] Subsynoptic polar mesoscale cyclones (or mesocyclones) are underrepresented in atmospheric reanalysis data sets and are subgrid scale processes in most models used for seasonal or climate forecasting. This lack of representation, particularly over the Nordic Seas, has a significant impact on modeled ocean circulation due to a consequent underestimation of atmospheric forcing at the air–sea boundary. Using Rankine vortices and a statistically significant linear relationship between mesocyclone diameter and maximum wind speed, a novel parameterization is developed that allows the bogusing in of missing or underrepresented vortices by exploiting a satellite-derived mesocyclone database. From October 1993 to September 1995, more than 2500 cyclones known to be missing from reanalysis data over the northeast Atlantic are parameterized into the forcing fields for a global ocean-only numerical modeling experiment. A comparison of this perturbed forcing simulation to a control simulation shows enhanced surface latent and sensible heat fluxes and a dramatic increase in the cyclonic rotation of the Nordic Seas gyre by four times the average interannual variability. In response to these changes, Greenland Sea Deep Water (GSDW) formation generally increases by up to 20% in 1 month, indicating more active open ocean convection. However such enhancements are smaller than the considerable monthly variability in GSDW production. An accompanying increase in the volume transport of intermediate and deep water overflowing the Denmark Strait highlights an important coupling between short-lived, intense atmospheric activity and deep ocean circulation. The parameterization scheme has the potential to be adapted for use in coupled climate models.

Citation: Condron, A., G. R. Bigg, and I. A. Renfrew (2008), Modeling the impact of polar mesocyclones on ocean circulation, *J. Geophys. Res.*, *113*, C10005, doi:10.1029/2007JC004599.

1. Introduction

[2] Wind stress and heat fluxes at the air–sea interface play an important role in driving surface and deep ocean circulation. In the Nordic Seas, the persistent loss of heat to the atmosphere during the winter months increases the density of the surface waters and gradually erodes the existing vertical stratification of the water column. Continual buoyancy losses during this period can eventually remove this stratification to allow localized regions of open ocean convection, in which surface waters sink to depth to form intermediate and deep waters [*Marshall and Schott*, 1999]. This water is then returned to the subpolar North Atlantic, via the Denmark Strait and/or the Faeroe-Shetland Channel (FSC), as the deep limb of the global meridional overturning circulation (MOC). Modeling studies indicate that the strength of the MOC is sensitive to volume transports from the Nordic Seas to the North Atlantic, and highlight that variations in the rate of vertical water exchange in the Nordic Seas can play a significant role in driving the global climate system [*Rahmstorf*, 1995; *Doscher and Redler*, 1997; *Bacon*, 1998].

[3] In order to understand the role of the atmosphere on deep water formation, and the strength of the MOC, it has become common practice in numerical ocean modeling to prescribe the state of the atmosphere using meteorological reanalysis data sets [*Hakkinen*, 1995; *Eden and Jung*, 2001; *Bigg et al.*, 2005]. These gridded data products are a comprehensive set of global analyses that describe the state of the atmosphere at regular time intervals over the last 10 to 50 years [*Kalnay et al.*, 1996; *Simmons and Gibson*, 2000]. Comparisons between atmospheric reanalysis data sets and in situ observations indicate that they tend to underestimate the intensity of the near-surface wind speed [*Kelly and Dickinson*, 1999; *Chelton et al.*, 2004; *Chelton and Freilich*, 2005], which will lead to inaccurate heat and momentum fluxes being prescribed at the air–sea boundary. It follows that in order to realistically force the underlying ocean, the representation of the air–sea fluxes prescribed must be accurate—a failure to capture both the number and

[1]Department of Earth, Atmospheric and Planetary Sciences, Massachusetts Institute of Technology, Cambridge, Massachusetts, USA.
[2]Department of Geography, University of Sheffield, Sheffield, UK.
[3]School of Environmental Sciences, University of East Anglia, Norwich, UK.

0148-0227/08/2007JC004599$09.00

magnitude of all atmospheric storm systems crossing the Nordic Seas will lead to an underforcing of the ocean.

[4] The accuracy of ocean models has been shown to improve with the inclusion of small-scale, high-frequency wind events in surface boundary layer forcing schemes. *Chen et al.* [1999] showed that by gradually increasing the resolution of satellite derived scatterometer data, the tropical Pacific Ocean cooled as a result of an increase in energy for vertical turbulent mixing. Similarly, *Kelly and Dickinson* [1999] observed an improved agreement in sea-surface height with satellite observations, and a response in the Sverdrup transport in the equatorial Pacific, when including high-frequency, small-scale wind in the forcing of a simple linear vorticity model. In the deep ocean, *Pickart et al.* [2003] highlighted a response in deep circulation to small spatial-scale atmospheric processes in a regional ocean-only model simulation of the mesoscale atmospheric Greenland tip jet that forms periodically in the lee of Cape Farewell. A lack of representation of this feature in the NCEP (National Centers for Environmental Prediction) reanalysis leads to the magnitude of the wind speeds, air–sea momentum and heat fluxes being considerably underestimated. However, following its parameterization, modeled air–sea heat fluxes over the Irminger Sea substantially increased the convective depth to 2000 m, in close agreement with observations.

[5] This paper focuses on a class of high-latitude, maritime weather systems known as polar mesocyclones, their representation in reanalysis data in the northeast Atlantic, and their potential effect on ocean circulation. It is worth noting that such systems are also generally subgrid scale for the atmospheric component of most coupled climate models, and so their impact is not well represented within climate modeling in general. Although polar mesocyclones are relatively small in size (typically 100–500 km in diameter) and short-lived (3–36 hours), observations by research aircraft reveal extremely high latent and sensible heat fluxes of greater than 500 W m^{-2} from the ocean to the atmosphere [see *Shapiro et al.*, 1987]. Furthermore, observations have shown a strong tendency for these vortices to cluster over the climatically important deep water convection region of the Nordic Seas [*Harold et al.*, 1999] (Figure 1a), suggesting that their overall effect on surface buoyancy may be substantial enough to encourage earlier or deeper convection, given regions of weakly stratified water.

[6] Recently, *Condron et al.* [2006] documented the number of polar mesocyclones in the European Centre for Medium-Range Weather Forecasts (ECMWF) atmospheric Reanalysis data (ERA-40). Using a cyclone detection algorithm, the authors located polar mesocyclones every 6 hours in mean-sea-level (msl) pressure from October 1993 to September 1995, and matched the position of each vortex detected against an existing data set of polar mesocyclones over the northeast Atlantic (50°–80°N, 50°W–50°E), previously observed from Advanced Very High Resolution Radiometer (AVHRR) satellite imagery by *Harold et al.* [1999, see also section 2c]. By comparing more than 3000 cyclonic cloud patterns to vortices located in the reanalysis data, it was shown that approximately 70–80% of systems with a diameter greater than 500 km were detectable in the msl pressure field (Figure 1b). However, this size category represents only 25% of the total number of mesocyclones observed in AVHRR satellite data (the remaining vortices are smaller). Below 500 km, an approximately linear decline in detection is observed, such that only 20% of systems with a 250-km-diameter are detectable in the reanalysis data. From this result, the authors conclude that the ERA-40 reanalysis is deficient in polar mesocyclones that have diameters below 500 km, and that as a consequence of this underrepresentation a substantial component of the associated air–sea heat and momentum fluxes will be missing when using this data set to force ocean models.

[7] In this paper we continue the work of *Condron et al.* [2006], and quantify the extent to which the ocean is underforced as a result of atmospheric reanalysis data failing to capture a large fraction of sub-500 km polar mesocyclones. We begin our analysis by comparing the spatial wind field patterns of two polar mesocyclones observed by research aircraft to wind velocity data from ERA-40. From our findings it is clear that the wind field, and also the momentum and heat fluxes in ERA-40 are all underrepresented during these events. Hence a parameterization to replicate the true magnitude of these fields in the reanalysis is developed and used to "enhance" the ERA-40 forcing fields, based on information from the satellite-derived database of *Harold et al.* [1999].

[8] An ocean-only global circulation model (OGCM) is run to examine the impact of this enhanced forcing over 2 years (October 1993 to September 1995), focusing in particular on the Nordic Seas. Changes in the Nordic Seas mixed-layer depth, air–sea heat flux, heat content, and volume transports across the Greenland-Iceland-Scotland (GIS) ridge, are all examined in response to the enhanced forcing. We conclude by discussing the importance for global ocean and climate modeling of forcing the ocean with an atmospheric resolution that is capable of capturing the magnitude of short-lived, but intense mesoscale atmospheric features.

2. Data Sets and Model Details

2.1. Reanalysis Data

[9] The ECMWF ERA-40 data set is a comprehensive set of global analyses describing the state of the atmosphere in 3 dimensions every 6 hours, from September 1957 to August 2002. The ERA-40 data assimilation system uses the Integrated Forecasting System (IFS) developed jointly by ECMWF and Météo-France, and has a T159 spectral resolution in the horizontal and 60 levels in the vertical [*Simmons and Gibson*, 2000]. The ECMWF ERA-40 surface data were available to us on a reduced Gaussian Grid, with 80 grid points aligned along the Greenwich Meridian from equator to pole, giving a north-south grid spacing of 1.125° (~125 km). In the east-west direction the grid point resolution varies with latitude; in the tropics 320 grid points produce a grid spacing of 125 km, while at 60°N and 70°N (in our study region) the grid point spacing gives a resolution of ~111 km and ~106 km, respectively. The smallest feature the ERA-40 spectral model can represent is, therefore, ~125 km in size [*Simmons and Gibson*, 2000]. However, for accurate representation and advection in a spectral model, features must be 2–4 times this smallest scale [see *Pielke*, 1991; *Laprise*, 1992]. For ERA-40, *Condron et al.* [2006] observe some representation of

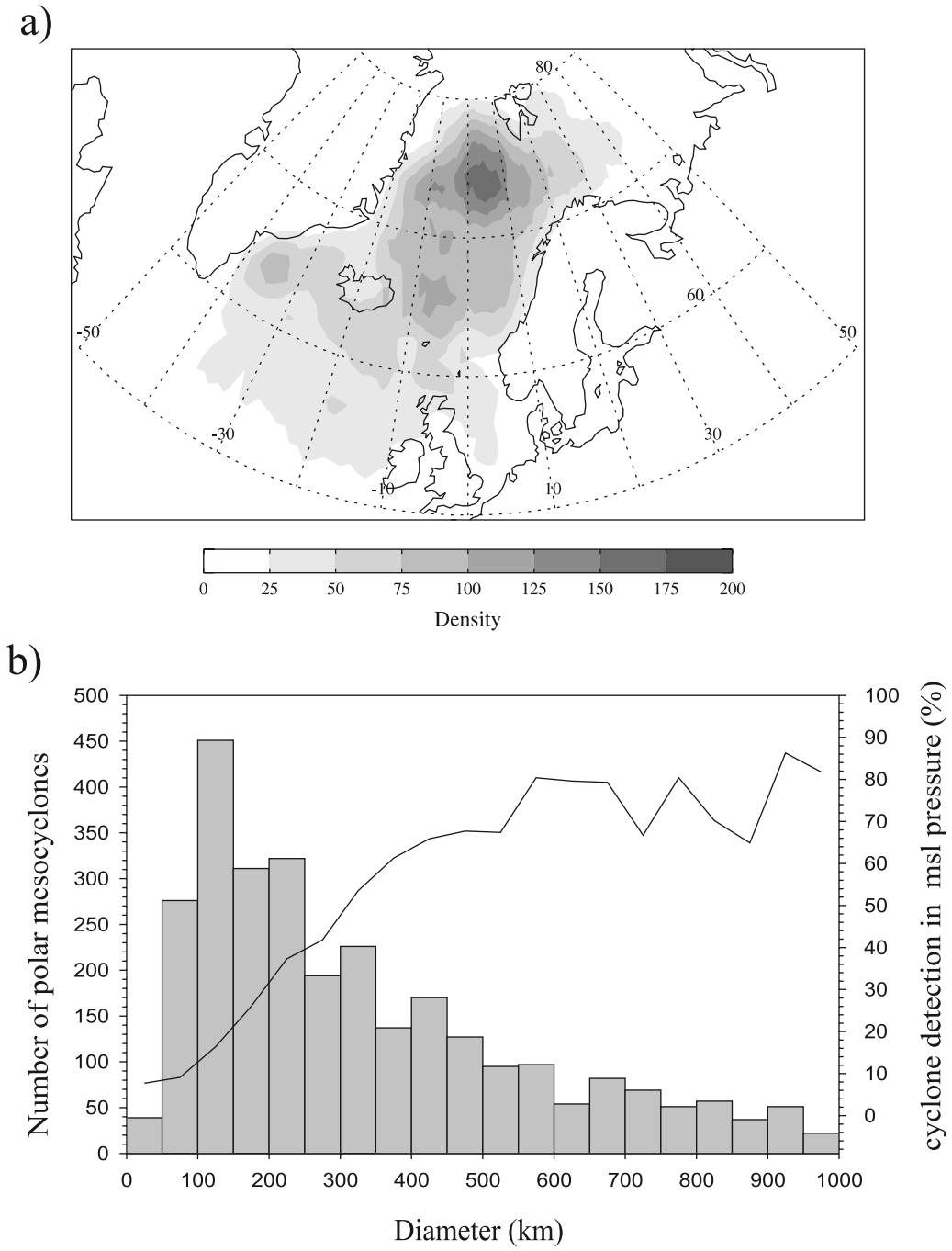

Figure 1. (a) The density of mesoscale cyclones as interpreted from AVHRR satellite images by *Harold et al.* [1999], given as the number of features per 125,000 km^2. Figure from *Condron et al.* [2006]. (b) The number of satellite observed cloud vortices in the northeast Atlantic (50°–80°N, 50°W–50°E) from October 1993 to September 1995 from *Harold et al.* [1999], per 50 km size category (gray shaded bars). Overlaid is the percentage of cloud vortices in each size group detectable in the ERA-40 msl pressure reanalysis data (solid black line). Figure modified from Figure 7 of *Condron et al.* [2006].

features of scale ~125–500 km, and a more consistent representation of features of scale >500 km (Figure 1b).

2.2. Satellite Wind Speed Data

[10] Wind speed data from the NASA QuikBird satellite microwave scatterometer data—so-called QuikScat data—are used to determine the maximum wind speed of 20 polar mesocyclones identified from AVHRR satellite data at the Norwegian Meteorological Institute in Tromso (Noer, unpublished data, 2005). The data are used in this paper to determine a relationship between maximum wind speed and vortex size (see section 4). The QuikScat data have a spatial resolution of 0.25° latitude by 0.25° longitude with an accuracy of ±1.7 m s^{-1} [*Chelton and Freilich*, 2005] and

are available twice daily since August 1999 from Remote Sensing Systems (www.remss.com). The lack of availability of this data set prior to 1999 meant that we could not use it to analysis the wind speed of vortices located in the *Harold et al.* [1999] satellite climatology.

2.3. Satellite Cloud Imagery

[11] A database of polar mesocyclones was compiled using AVHRR (11 μm infrared) satellite imagery from 1 October 1993 until 30 September 1995 by *Harold et al.* [1999] over the northeast Atlantic. In order to be consistent with *Condron et al.* [2006] we restrict the *Harold et al.* [1999] data set to the 5370 mesoscale cloud patterns observed in more than one satellite image, as these are most likely to significantly impact upon the ocean and be assimilated into the reanalysis. The vortices observed had a continuous spectrum of diameters below 1000 km, but with a distribution skewed toward smaller diameters, as illustrated by a modal size of 100–150 km (see Figure 1b).

2.4. Details of the Ocean Model

[12] The global ocean general circulation model is a hydrostatic three-dimensional finite difference primitive equation model that is based on the Modular Ocean Model (MOM) code [*Bryan*, 1969; *Semtner*, 1974; *Cox*, 1984], with the model equations found in *Beare* [1998]. The model has 182 $\times$ 211 grid points in the zonal and meridional directions, respectively, and is a finer resolution version of the global curvilinear coordinate system model developed by *Wadley and Bigg* [2002]. A free surface formulation is used for the barotropic mode, and there are 19 levels in the vertical that vary in thickness from 30 m at the surface to 500 m at depth. To enhance the model grid resolution in the North Atlantic the North Pole is located in Greenland (72.5°N, 40°W), producing a resolution in the Irminger and Nordic Seas of approximately 50 km. The time-step length is a function of grid spacing, with the coarsest time step being 2700 s and the shortest, along the Greenland coast, being an eighth of this [*Wadley and Bigg*, 2002].

[13] Tracer salinity and temperature mixing coefficients are taken from *England* [1993], with the exception of the horizontal mixing coefficient, which was decreased to 1×10^8 cm^2 s^{-1}. The horizontal momentum diffusivity varies with grid resolution [*Wadley and Bigg*, 2002], while the near surface vertical mixing uses the scheme of *Pacanowski and Philander* [1981]. A one-layer thermodynamic sea-ice model is also coupled to the OGCM. Ice growth is based upon the thermodynamic growth model of *Parkinson and Washington* [1979], while sea ice transport is a simplified version of the *Flato and Hibler* [1992] sea-ice model, in which ice advection is only a function of ocean current velocity.

[14] The model was spun-up to equilibrium over 50 years with surface boundary conditions prescribed by monthly ERA-40 climatological (av. 1979–1999) reanalysis heat (longwave, shortwave, latent and sensible) fluxes, freshwater and momentum flux. The net freshwater flux is derived from the difference between the total precipitation and evaporation, with evaporation calculated by dividing the latent heat flux by the latent heat of vaporization.

[15] After the spin up, a control run was created by forcing the model for 3 years with 6-hourly ERA-40 reanalysis data from 1 January 1993 to 31 December 1995 so as to overlap the mesocyclone climatology of *Harold et al.* [1999]. Wind stress and latent and sensible heat fluxes were calculated every 6 hours using standard bulk aerodynamic formulae based on those implemented in the ECMWF model, and using relative humidity, 2 m air temperature, and 10 m wind velocity from ERA-40, and sea surface temperatures taken from the top level of the ocean model. The mean Atlantic meridional overturning circulation (MOC) strength in the control integration is 20.3 Sv, and close to observational values of ~18 Sv [see, for example, *Wunsch*, 2005; *Cunningham et al.*, 2007]. A second perturbed run was created in which polar mesocyclones determined to be absent from the reanalysis by *Condron et al.* [2006] were "bogused" into the atmospheric forcing fields via a mesocyclone parameterization—as detailed in the following sections.

3. The Representation of Two Mesocyclones in ERA-40

[16] During the late 1980s, investigations into the three-dimensional structure of several polar mesocyclones over both the Nordic Seas and Gulf of Alaska were made from research aircraft [*Shapiro et al.*, 1987; *Douglas et al.*, 1991, 1995]. In this paper we report on two vortices that occurred over the Nordic Seas, while two additional vortices that occurred over the Pacific Ocean and Barents Sea examined in *Condron* [2007] are also referred to here.

[17] The first aircraft observations were made within an intense polar mesocyclone just south of Jan Mayen Island at 68°N, 2°W in the Norwegian Sea during the Arctic Cyclone Expedition (ACE), on 27 February 1984 [*Shapiro et al.*, 1987]. The system developed in conditions somewhat typical for polar mesocyclone development [see, for example, *Rasmussen and Turner*, 2003], forming toward the rear of a larger synoptic cyclone in a region of strong baroclinicity that was associated with an outbreak of cold air from Greenland, and an upper-level eastward propagating short wave. Satellite imagery at 1341 UTC shows a ~400-km-diameter cloud structure associated with the polar mesocyclone during its mature phase, revealing an ~80-km-diameter cloud-free inner eye, somewhat similar to that of a tropical cyclone (Figure 2a).

[18] The second polar mesocyclone examined formed at the east Greenland ice edge on 18 March 1989, during the Coordinated Eastern Arctic Research Experiment (CEAREX) [*Douglas et al.*, 1995]. Once again, the polar mesocyclone developed in a cold arctic-air outbreak that was associated with an upper-level trough at the 500-hPa geopotential height level. The vortex had a comma cloud pattern, and persisted for 40 hours, during which time it also had an average diameter of ~400 km (Figure 2b).

[19] The series of low-level flight passes through the ACE and CEAREX polar mesocyclones document a very similar structure in both cases. The near-surface wind speed increases outward from a minimum at the center, toward a maximum in the main convective cloud shield, revealing a pattern somewhat similar to tropical hurricanes [*Haurwitz*, 1951]. The ACE vortex was observed to be the more intense of the two systems, with maximum wind speeds >30 m s^{-1},

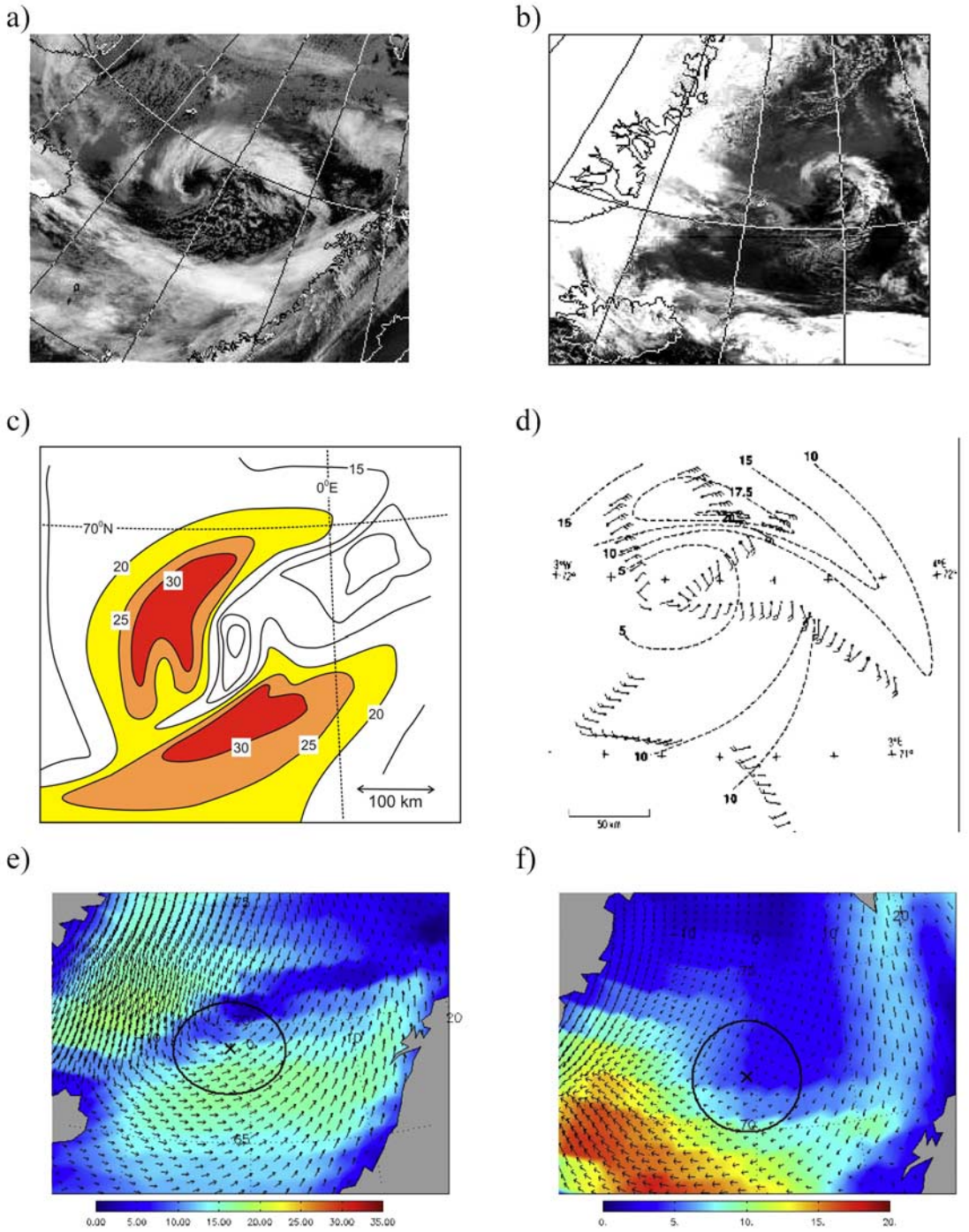

Figure 2. (a–b) Satellite imagery, (c–d) aircraft wind speed observations, and (e–f) ERA-40 wind fields for the ACE (a, c, e) and CEAREX (b, d, f) polar mesocyclone. (a–b) AVHRR infrared satellite image taken at (a) 1341 UTC 27 February 1984 and (b) at 1748 UTC 18 March 1989. (Images courtesy of the NERC Satellite Receiving Station, University of Dundee). (c–d) Wind speed (m s^{-1}) observed from aircraft observations from approximately 960 hPa at (c) 1340 UTC 27 February 1984 [after *Shapiro et al.*, 1987] and (d) 1255 UTC and 1518 UTC 18 March 1989 [taken from *Douglas et al.*, 1995]. (e–f) ERA-40 wind speeds (m s^{-1}) interpolated onto the ocean model grid at (e) 1200 UTC 27 February 1984 and (f) 1800 UTC 18 March 1989. The color shading shows the wind speed (m s^{-1}), while black vector arrows indicate the wind direction at each grid point; black crosses the center of each vortex, and the thick black line its outer edge.

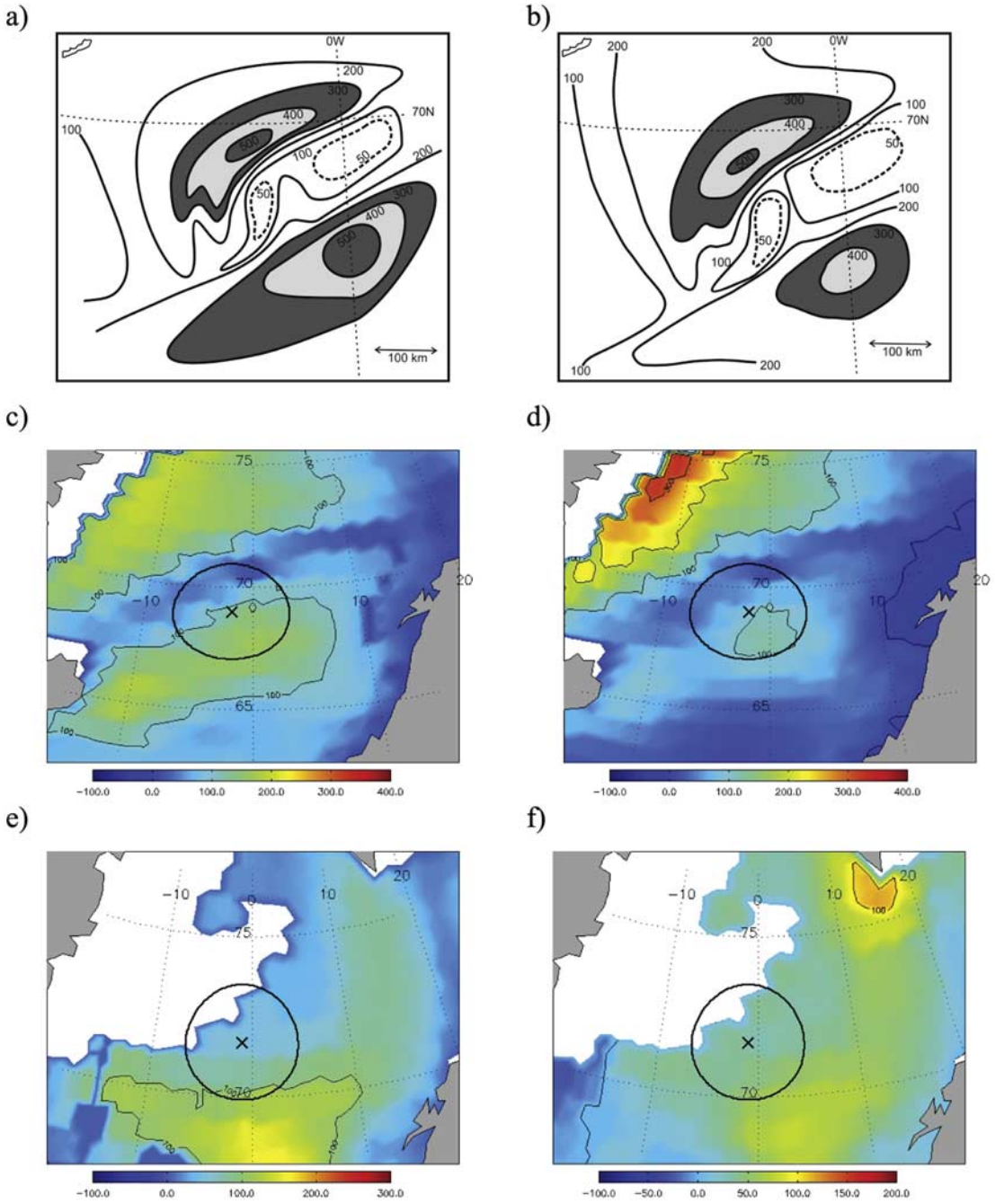

Figure 3. The air–sea (a) latent (b) sensible heat flux (W m^{-2}) observed by *Shapiro et al.* [1987]. Solid (dashed) lines represent an upward (downward) air–sea heat flux. (c, e) Latent and (d, f) sensible heat fluxes from ERA-40 for the (c–d) ACE and (e–f) CEAREX vortices. White denotes sea ice in Figures 3c–3f.

compared to only 20 m s^{-1} for the CEAREX vortex (Figures 2c and 2d).

[20] The wind speed and direction from the 6-hourly ERA-40 reanalysis periods closest to the aircraft observations are shown in Figures 2e and 2f. Despite the closest reanalysis period at 1200 UTC 27 February 1984 (approximately 1 hour 47 minutes before the satellite picture in Figure 2a), capturing the general synoptic setting of the ACE vortex very well, there is no representation of the mesoscale flow associated with the vortex. Consequently, the maximum wind speeds at this time in the reanalysis are only 17.3 m s^{-1}; about half of those observed by *Shapiro et al.* [1987] (Figure 2c). Figure 2f illustrates a similar underrepresentation in the winds in the closest reanalysis time to the CEAREX vortex at 1800 UTC 18 March 1989. Although the synoptic-scale setting is well resolved, there is no evidence of any mesoscale structure at this time—the maximum wind speed is only 9.9 m s^{-1}, that is about half

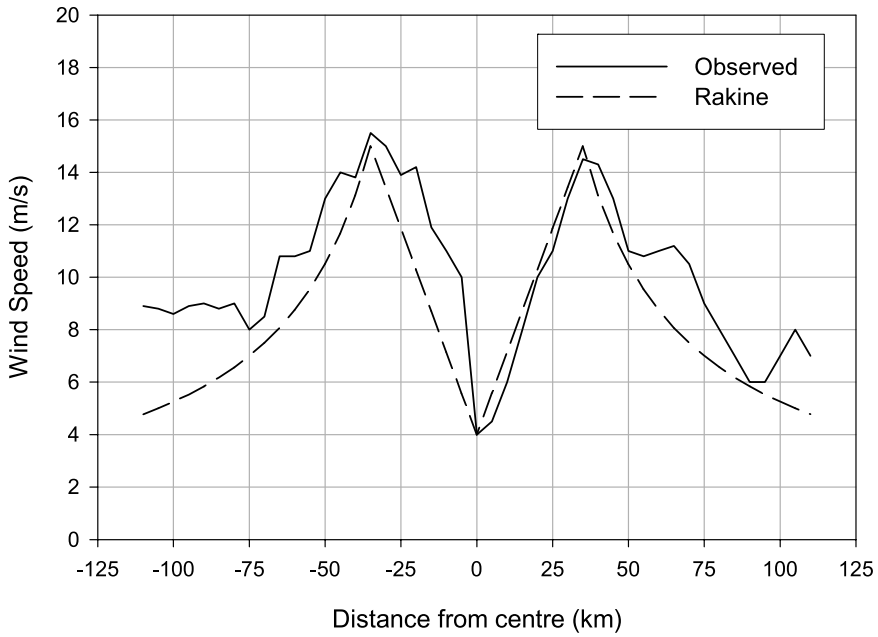

Figure 4. Wind speed modeled as a Rankine vortex and observed wind speed data of a polar mesocyclone investigated by *Rasmussen et al.* [1992].

the value observed from aircraft observations. Such an underrepresentation of wind velocities in mesocyclones in reanalyzes is also documented in *Condron* [2007] for a polar mesocyclone over the Gulf of Alaska [see *Douglas et al.*, 1991] and a case over Bear Island in the Barents Sea [see *Rasmussen et al.*, 1992].

[21] Using bulk aerodynamic flux formula, *Shapiro et al.* [1987] calculated high air–sea latent and sensible heat fluxes from the ocean to the atmosphere during the ACE polar mesocyclone due to relatively cold, dry air passing over the ocean. Total values were determined to be over 1000 W m^{-2}, although individually fluxes of latent and sensible heat were typically on the order of 200–300 W m^{-2} (Figures 3a and 3b). In contrast, the average latent and sensible heat fluxes in the ERA-40 data set in the vicinity of the vortex are 94 W m^{-2} and 66 W m^{-2}, respectively, with maximum values of 161 W m^{-2} and 134 W m^{-2} (Figures 3c and 3d); about three times lower than instrumental observations suggest. Although *Douglas et al.* [1995] did not make any heat flux calculations for the CEAREX vortex, we use bulk formula to estimate maximum latent and sensible heat fluxes of 250 and 260 W m^{-2}, respectively, by taking a maximum observed wind velocity of 20 m s^{-1} and humidity, sea surface temperature and air temperature from ERA-40 at 1800 UTC 18 March 1989. These values compare to maximum fluxes in the ERA-40 data set of 119 W m^{-2} and 63 W m^{-2}, respectively—approximately 2–4 times lower than observations suggest (Figures 3e and 3f).

[22] The inability of the reanalysis data to accurately reproduce the near-surface wind speed and air–sea heat fluxes for these two cyclones highlights a considerable deficiency in the magnitude of the fluxes being prescribed at the air–sea interface. The underestimation of the wind field not only results in heat fluxes being lower than observed, but also leads to a reduced estimate of the surface momentum flux, with clear consequences for currents, at least in the short term, as discussed further in section 6.

[23] Of particular note at this point in the discussion is our finding that both of the cases discussed above are detectable disturbances in the ERA-40 msl pressure field using the cyclone tracking algorithm of *Murray and Simmonds* [1991] and the method of *Condron et al.* [2006]. So despite neither of these vortices being well-represented in the ERA-40 wind field, they are (weakly) included in the atmospheric reanalysis. This is also the situation for the other two cases documented by *Condron et al.* [2006]—the Gulf of Alaska and Barents Sea cases. This finding has significant repercussions for the number of polar mesocyclones one should parameterize at the air–sea boundary, that is, the extent to which mesocyclonic forcing is being underrepresented in the reanalysis. *Condron et al.* [2006] found that 40% of vortices observed from satellite imagery with a diameter of 400–450 km were associated with a low pressure signature in the reanalysis (Figure 1b), and as such one may have expected the detectable fraction to capture the mesoscale characteristics of the polar vortex. However, the above cases suggest that the ERA-40 data set also underrepresents the winds associated with the mesocyclones that are detected. Indeed it suggests that all vortices with a diameter below 500 km require an "enhancement" in order for an accurate representation, and an accurate forcing field for the ocean model. In the next section we discuss a parameterization that attempts to mimic the wind field associated with individual polar mesocyclones and, in so doing, enhances the air–sea momentum and heat fluxes to produce a more realistic atmospheric forcing of the ocean.

4. Developing a Mesocyclone Parameterization

[24] The two-dimensional velocity structure of a polar mesocyclone can be described by a Rankine combined

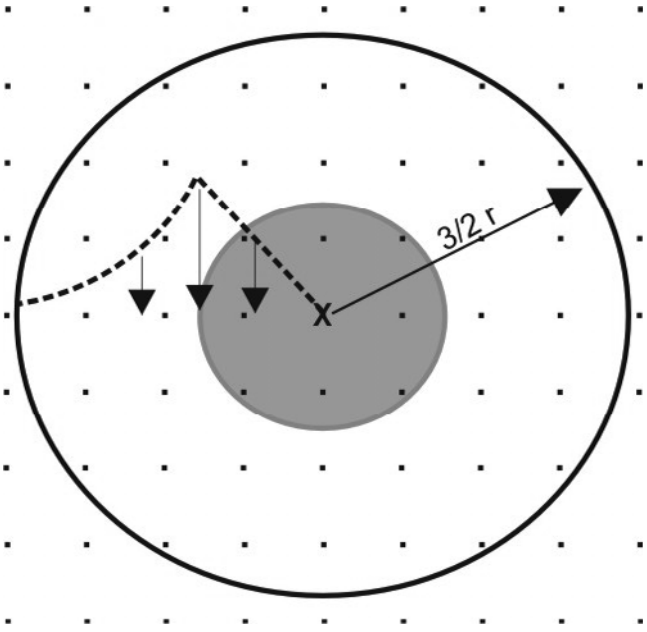

Figure 5. An example of how the gridded wind field data are altered by adding a Rankine vortex. All grid points within the black circle centered at "x" are perturbed. Those grid points within the gray circle are in solid body rotation. The bold dashed black line shows the idealized wind profile and the arrows the flow direction, both due west of the center. Black dots indicate grid points.

vortex (for a detailed description of a Rankine vortex, see, for example, *Batchelor* [1967]), and was used by *Renfrew et al.* [1997] to consider the binary interaction of these vortices. The prescription of a polar mesocyclone as a Rankine vortex is also in good agreement with the wind field structure observed as a polar mesocyclone tracked across Bear Island (74°N, 19°E) in the Barents Sea between 1100 and 1900 UTC 15 December 1982 [*Rasmussen et al.*, 1992]. Figure 4 illustrates the similarity of the observed wind speed to the velocity distribution of a Rankine vortex.

[25] The Rankine vortex rotates about a fixed axis with an inner core in solid body rotation, that is, with constant relative vorticity (Figure 5). Hence its wind speed increases linearly from the center to a region of maximum wind, and then decreases inversely with distance to the edge of the vortex. In the mesocyclone cases examined here, the edge of the vortex is defined as the outer edge of the main cloud band [*Harold et al.*, 1999]. The velocity profile, U_R, is defined as:

$$U_R = U_M \frac{r}{R_M}, r < R_m \tag{1a}$$

$$U_R = U_M \frac{R_M}{r}, r > R_m \tag{1b}$$

where r is the radial distance of the vortex, U_M is the maximum wind speed, and R_M is the radius of maximum wind speed. The radius of maximum wind speed is taken to be half the total radius of a vortex observed on satellite imagery. In this study, the radius of maximum wind speed, R_M is taken to be half the total radius, r, of any vortex identified by *Harold et al.* [1999].

[26] To include the Rankine vortex within the existing ERA-40 wind field a technique commonly used in Numerical Weather Prediction (NWP) known as "bogusing" is used [*Kurihara et al.*, 1993; *Singh et al.*, 2005]. The method is typically used when the magnitude of a numerically modeled low-latitude tropical storm is too weak, compared to observations. The cyclone is initially replicated as a Rankine vortex of equivalent size, and then placed within the original simulated wind field at the correct location to create a vortex that has wind speeds in closer agreement with observations. We now describe this in terms of its application to parameterizing polar mesocyclones in reanalysis data.

[27] Initially, the closest grid point to the latitude and longitude of the vortex being included is located, and this becomes the new center of the vortex. A search is then carried out for all grid points that are less than or equal to 3/2 times the satellite-determined radius of the vortex. This is introduced to avoid perturbing beyond the bounds of the mesocyclone (Figure 5). The wind speed of each grid point that is less than R_M from the centre of the vortex is increased in solid body rotation to a perturbed maximum (U_M) using equation (1a), while grid points beyond the region of maximum wind speed are perturbed using equation (1b). A cyclonic rotation is imposed upon the vortex by calculating an angle 90° to the left of the line between each grid point and the centre of the vortex. The resultant zonal and meridional wind speeds are then derived by adding the perturbed wind speed and direction to the existing ERA-40 wind field:

$$\begin{aligned} U'_{10} &= U_R \sin\phi + U_{10} \\ V'_{10} &= U_R \cos\phi + V_{10} \end{aligned} \tag{2}$$

where ϕ is the wind direction in the Rankine vortex, U_R is the perturbed wind speed at a particular grid point, U_{10} and V_{10} are the ERA-40 zonal and meridional wind components, and U'_{10} and V'_{10} are the new perturbed zonal and meridional wind components.

[28] If the ERA-40 data are interpolated to the grid of our ocean model (as is done each time new data fields are read into the model) it is possible to represent, to some extent, vortices with a diameter of only ~50 km in the Greenland Sea. However, at this scale only one grid point from the vortex center will be perturbed, and therefore the feature will not be fully resolved. We find that vortices with a diameter of 120 km (or more) will be fully resolved by our parameterization, while vortices with a diameter 50–120 km will only be partially resolved in our model for this region.

[29] There are not observed wind speed data associated with the polar mesocyclones observed by *Harold et al.* [1999], which makes it difficult to prescribe a value for the maximum wind speed (U_M). We overcome this shortcoming by developing a novel size-wind speed relationship to allow U_M to be approximated for all polar mesocyclones, based only on the size of each vortex. To the best of our

Table 1. The Maximum Wind Speed (m s^{-1}) and Diameter (km) of 24 Polar Mesocyclones Observed Over the North Atlantic[a]

ID No.	Date	Time (UTC)	Lat. (°N)	Long. (°E)	Diameter (km)	Max. wind speed (m s^{-1})
1	19.12.1999	1340	72	18	260	19.6
2	22.01.2000	0250	72.5	29	160	15.4
3	31.01.2000	0610	65	4	460	27.0
4	24.03.2000	1230	72.5	21	340	18.4
5	04.02.2001	1540	62.5	357	510	19.4
6	05.02.2001	1600	65	359	300	23.6
7	24.03.2001	0730	74.5	9	320	15.4
8	10.04.2001	0650	72	2	460	43.0
9	01.11.2001	0200	71	19	480	41.0
10	12.11.2001	0700	67.5	7	430	33.4
11	12.01.2002	1200	73	21	320	24.5
12	19.01.2002	0400	70	47	250	14.0
13	22.01.2002	1100	72	15	180	15.8
14	19.02.2002	1300	74	36	380	27.4
15	23.02.2002	1140	67.5	7	230	14.6
16	05.05.2002	0850	75.5	10	250	18.4
17	20.05.2002	1615	75	7	240	10.0
18	16.01.2003	1400	72	7	460	29.6
19	17.01.2003	0000	73.5	25.5	210	20.0
20	29.01.2003	0700	73.5	0.5	450	23.0
Norwegian Sea[b]	27.02.1984	1341	68	358	400	35.0
Alaskan low[c]	23.03.1987	1822	58.5	145	300	15.0
Greenland[d]	18.03.1989	1748	72	358	400	17.5
Bear Island[e]	15.12.1982	1400	74	19	150	15.0

[a]The maximum wind speed for each vortex is determined from QuikScat data for 1–20 and from in situ observations for the named cases. Vortices 1–20 were observed by Noer [unpublished data, 2005] at the Norwegian Meteorological Institute in Tromso.
[b]*Shapiro et al.* [1987].
[c]*Douglas et al.* [1991].
[d]*Douglas et al.* [1995].
[e]*Rasmussen et al.* [1992].

knowledge, no such relationship has previously been established.

[30] Using QuikScat data we determine the maximum wind speed associated with 20 polar mesocyclones recently identified from AVHRR satellite imagery [Noer, unpublished data, 2005]. This is achieved by taking the closest QuikScat image to the occurrence time of each AVHRR observed polar mesocyclone, and then performing a search in the QuikScat data for the maximum wind speed in all data points that are a distance less than 3/2 the radius of each vortex from its center (Table 1). To increase the sample size we also include the 4 case studies discussed above; two of which are from the previously discussed aircraft case studies, the third from the polar mesocyclone tracking over Bear Island between 1100 and 1900 UTC 15 December 1982 (shown in Figure 4), and the final vortex from observations by *Douglas et al.* [1991] of the mesocyclone tracking over the Gulf of Alaska [as discussed in *Condron*, 2007].

[31] Figure 6 illustrates a clear relationship between vortex size and maximum wind speed. There is a Pearson product moment *r*-value of +0.7 that is statistically significant at the 99.9% confidence level [*Shaw and Wheeler*, 2000] and is indicative of larger vortices having higher maximum wind speeds. The relationship suggests a parameterization of the maximum wind speed U_M:

$$U_M = 0.1114r + 3.897 - U_{CT} \quad (3)$$

where r is the radius of the vortex (in km), and U_{CT} is the existing wind field in the reanalysis data at the center of the vortex. This relationship is limited by the sizes of the vortices to the range ~100–500 km in diameter. Clearly such a linear relationship would not hold for indefinitely

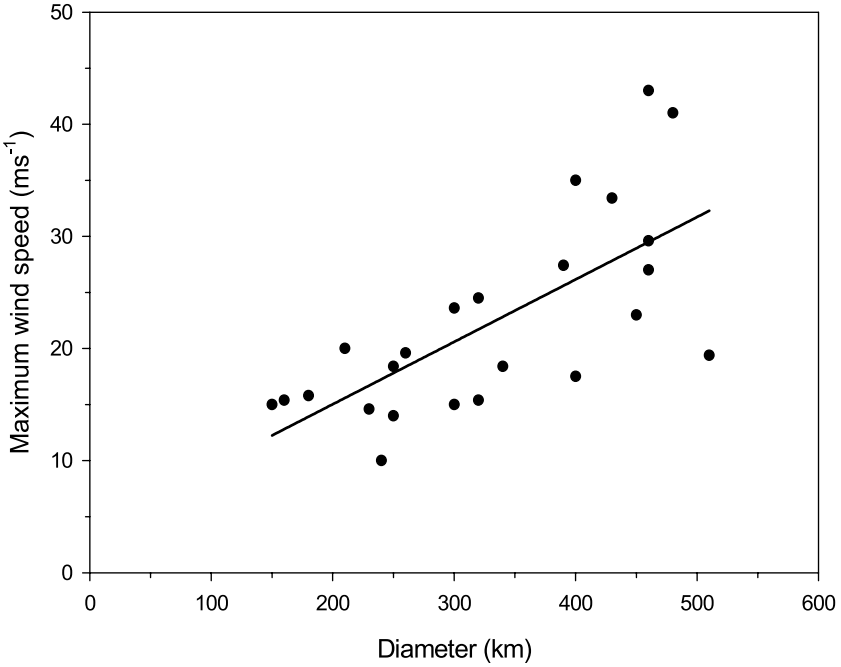

Figure 6. The relationship between polar mesocyclone size (km) and maximum wind speed (m s^{-1}), U_M, for 24 examples. A linear regression is added to highlight the relationship (solid black line), giving an *r*-value of $r = 0.7$ that is statistically significant at the 99.9% confidence level.

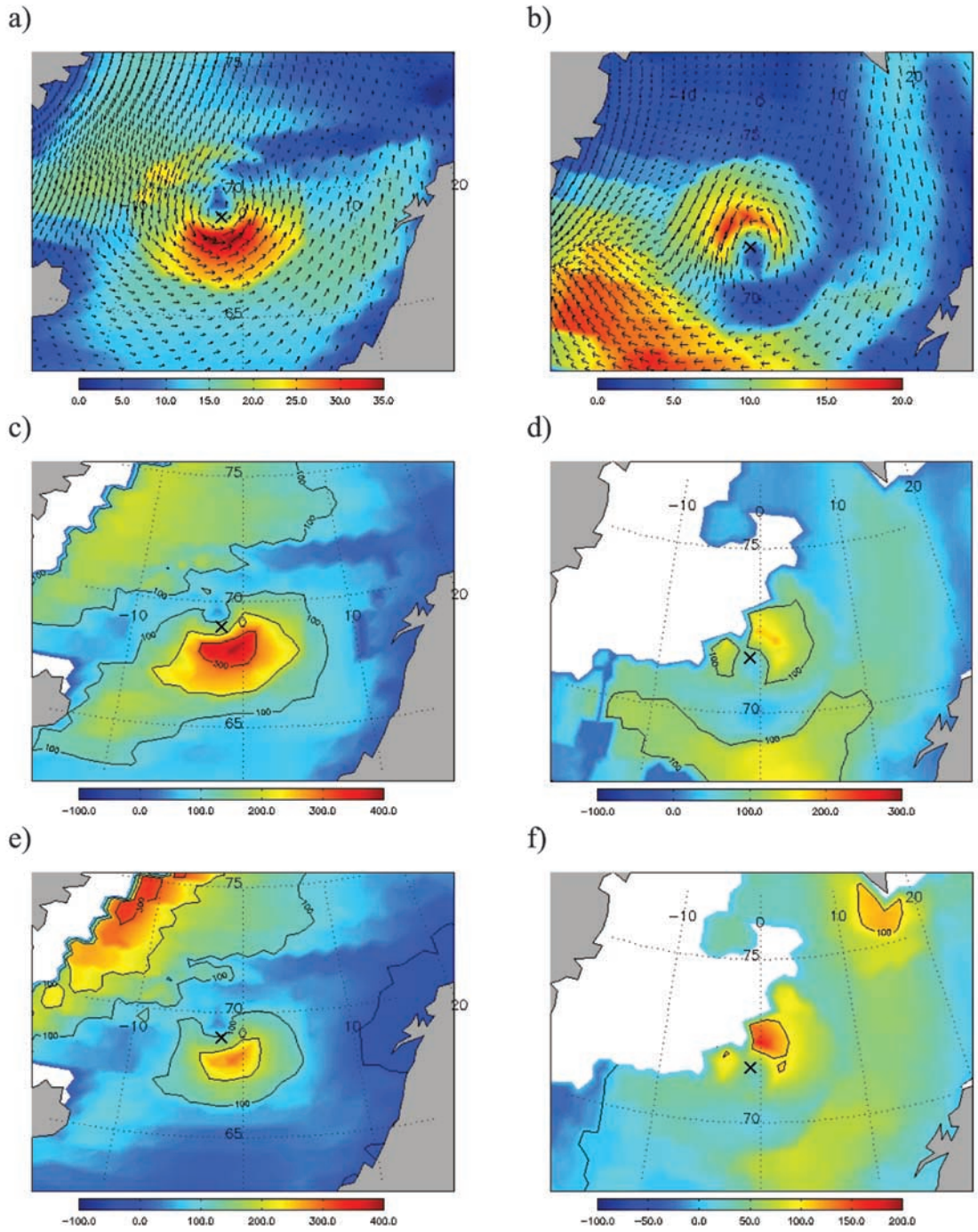

Figure 7. (a–b) The perturbed wind speed (m s^{-1}), latent (c–d) and sensible (e–f) heat flux (W m^{-2}) for the ACE (a, c, e) and CEAREX (b, d, f) mesocyclones following the bogusing of each vortex. Black contour lines intervals are 100 W m^{-2}, and white denotes is sea ice in Figures 7c–7f.

large cyclones and we would emphasize we only use it for mesocyclones below 500 km in size. Fortunately *Condron et al.* [2006] show that the ERA-40 reanalysis captures up to 80% of vortices with a diameter greater than 500 km, with no improvement in capture rate with size beyond this diameter (see also Figure 1b), and as a result we choose not to parameterize mesocyclones >500 km in diameter.

[32] To validate the parameterization we bogus the wind field of the ACE and CEAREX polar mesocyclones (previously shown in Figures 2 and 3) and compare the perturbed representation with the original observations. The addition of a Rankine vortex to the existing ERA-40 wind field in the location of the ACE mesocyclone captures the cyclonic circulation structure of this vortex extremely effectively, producing wind speeds in remarkable agreement with those observed by *Shapiro et al.* [1987] and a very similar velocity structure—compare Figure 7a and Figure 2c. The highest perturbed wind speeds of 35 m s^{-1} are observed

on the southwest flank, while the lower wind speeds to the northeast are a result of the general west-south-west background flow in this location. Parameterizing the wind field also enhanced the surface momentum flux, with average values increasing from 0.4 N m^{-2} to 1.3 N m^{-2}. The additional cyclonic rotation at the air–sea boundary will also increase cyclonic stirring—a pattern that appeared to be observed under the ACE vortex [*Shapiro et al.*, 1987].

[33] Recalculating the heat flux using the perturbed wind field depicted in Figure 7a (and keeping all other variables the same) significantly increased both the latent and sensible heat fluxes, with average fluxes of 163 and 115 W m^{-2}, respectively; approximately 1.7 times the magnitude of the fluxes previous observed (Figures 7c and 7e). The largest fluxes correspond to the region of maximum wind speed, and produce latent and sensible heat fluxes of 387 W m^{-2} and 292 W m^{-2}, respectively, and a total maximum heat flux of ~650 W m^{-2}. Unlike the observations (Figures 3a and 3b), however, the spatial pattern of the heat fluxes to the north of the vortex are too weak. This is partly the result of the perturbed wind field being weaker than observations here, but we also note that even where the wind fields are the same, heat fluxes continue to be lower than observations. Hence, it is likely that the air temperature and specific humidity in ERA-40 are not representative of this mesocyclone either. Despite this, it is reassuring that the pattern is well represented and the magnitude compares reasonably well.

[34] Parameterizing the CEAREX vortex also yields encouraging results. The parameterized wind field exhibits a strong cyclonic circulation that is in good agreement with observations, with a maximum wind speed of 17.4 m s^{-1} (only 2.6 m s^{-1} less than observations) in the main cloud band to the north of the center. Lower wind speed values are observed to the south of the vortex center as a result of an easterly background flow in this region. In line with the increase in wind speed, the momentum flux (not shown) increased from an average of ~0.2 N m^{-2} to over 0.3 N m^{-2}, with maximum values increasing from 0.4 N m^{-2} to 0.8 N m^{-2}. Recalculating the heat fluxes using the perturbed wind field resulted in average latent and sensible heat fluxes of 76 and 51 W m^{-2}, respectively, which again are approximately 1.7 times the original ERA-40 fluxes (Figures 7d and 7f). The largest fluxes correspond to the region of maximum wind speed, with latent and sensible heat fluxes peaking at 183 W m^{-2} and 159 W m^{-2}, respectively, producing values 1.5 and 2.5 times those previously observed in this region. These upper values are less than those estimated in section 3 due to the maximum wind speed being lower (17.4 m s^{-1}) than the 20-m s^{-1} used in our previous calculation.

5. Including Vortices in the Atmospheric Forcing Fields

[35] To investigate the impact of polar mesocyclones on ocean circulation we parameterized the 2 years of mesocyclone activity observed in the northeast Atlantic by *Harold et al.* [1999] in the ERA-40 reanalysis wind field, using the methods previously described, creating new forcing fields for the perturbed run. As the model stepped forward in time from January 1993 to December 1995, ERA-40 reanalysis data fields were read in every 6 hours (0000, 0600, 1200, 1800 UTC). At each time step, a search was carried out in the *Harold et al.* [1999] climatology of satellite observed polar mesocyclones to determine the number of vortices that needed to be included within the forcing at this time. Vortices were only selected for inclusion at a given time step if they were observed within ±3 hours of the reanalysis time. To compensate for infrequent satellite passes within ±3 hours of 0000 UTC, the size and position of individual vortices was interpolated between 1800 UTC and 0600 UTC the following day, provided the vortex still existed. Occasionally, no size and position data were available at 1800 UTC, despite the vortex being present both at 1200 UTC and then 0600 UTC the following day. In this instance, the size and position of the vortex at 1800 UTC and 0000 UTC were obtained by interpolating between 1200 UTC and 0600 UTC the following day.

[36] The observed lack of mesocyclonic representation in the near-surface wind field in ERA-40, despite a surface disturbance frequently being detectable in the msl pressure field (section 3), lead us to include *all* multisighted vortices observed by *Harold et al.* [1999] with a diameter less than 500 km, in the ocean model forcing. As a result, 2605 vortices were bogused in, at the correct time and position, from October 1993 to September 1995 to create the forcing for the perturbed run; this is equivalent to ~3.5 weather systems per day.

6. Results

[37] We begin our analysis by examining the difference in wind speed, heat flux, and the physical properties of the water in the Nordic Seas region for the control and perturbed runs. The Nordic Seas are defined as the area north of Iceland to the Fram Strait, and east of Greenland to the Barents Sea (65°–80°N, 20°W–20°E). The difference between the control and perturbed runs are always calculated as the perturbed run minus the control run.

[38] The average wind speed in the control run for the 2-year period is 7.73 m s^{-1}, while higher values of 9.25 m s^{-1} and 10.14 m s^{-1} are observed during winters (DJFM) 1993/94 and 1994/95, respectively, in response to the seasonal intensification of the North Atlantic storm track. The higher winter wind speeds observed during the second winter are a result of the occurrence of the second highest positive phase of the North Atlantic Oscillation (NAO) index recorded in the last 50 years (the highest being 1989) [*Hurrell*, 1995].

[39] The average wind speeds over the Nordic Seas in the perturbed run are higher than in the control run. Over the 2-year study period, the wind speed was observed to increase by 0.1 m s^{-1} (on average), and by 0.18 m s^{-1} and 0.12 m s^{-1} for the first and second winters, respectively. The impact of the parameterization is best observed by examining the maximum wind speed over the Nordic Seas every 6 hours, from October 1993 to September 1995 (Figure 8a). Here the effect of resolving individual mesocyclonic storm systems is clearly visible due to the higher wind speeds imposed on the surface of the ocean, compared to the standard ERA-40 wind field. The largest difference in maximum wind speed observed between the control and perturbed runs was 29.6 m s^{-1} and resulted from parameterizing a large (~481 km in diameter) polar mesocyclone

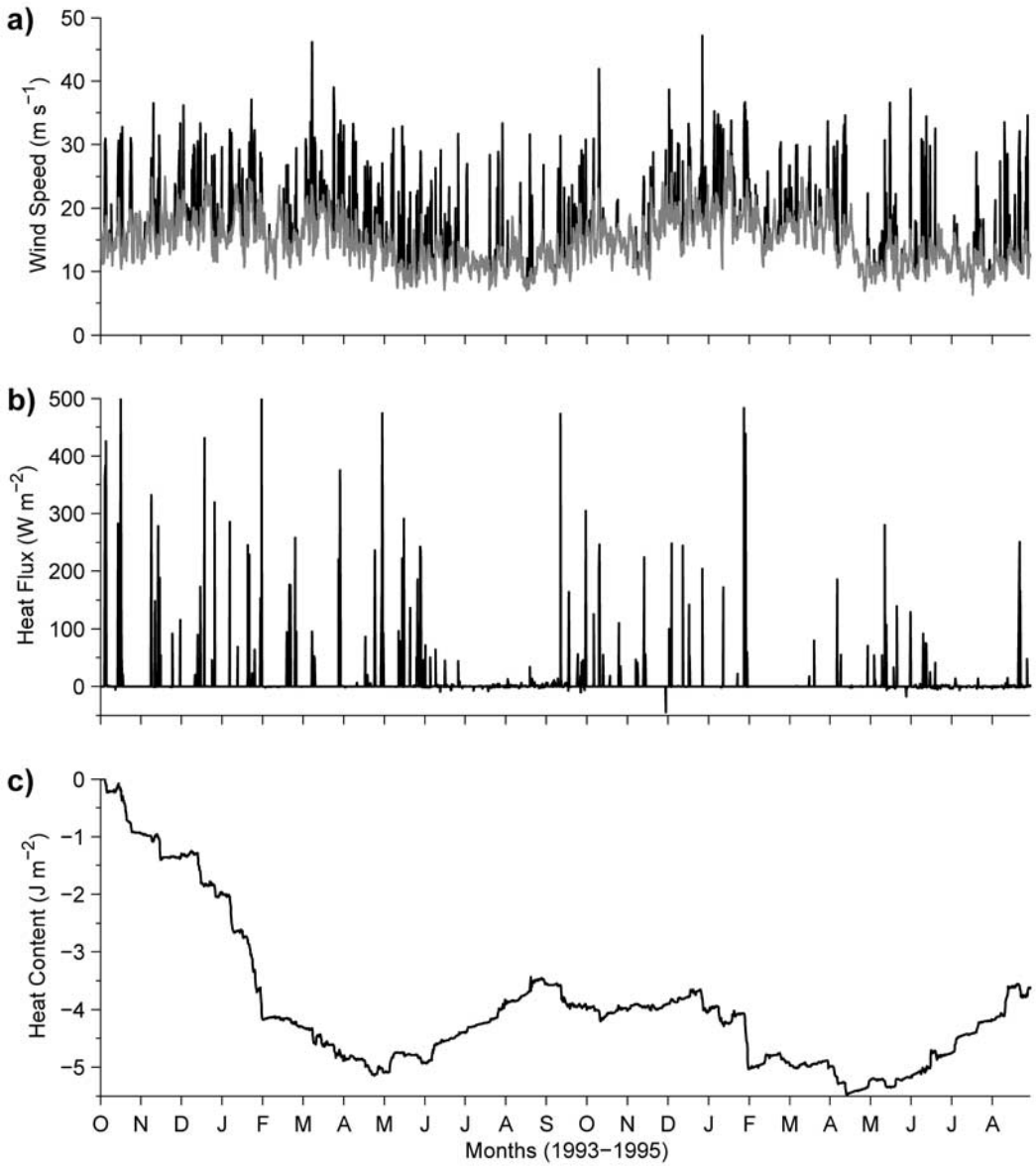

Figure 8. (a) The maximum surface wind speed for the control (gray) and perturbed (black) runs. (b) The total (latent + sensible) heat flux (W m^{-2}), and (c) ocean heat content difference between the two runs (10^{10} J). All data are shown for the Nordic Seas region (65°–80°N, 20°W–20°E) every 6 hours, from October 1993 to September 1995.

in the northern Nordic Seas, at approximately 71°N, 8°E, on the 28 December 1994, where previously this event had not been resolved.

[40] The annual and seasonal variability in air–sea latent and sensible heat fluxes over the Nordic Seas are correlated to the changes in wind speed, as a result of using bulk formulae for the heat fluxes. The total (latent + sensible) annual mean heat flux over the Nordic Seas remains positive for the 2 years, while larger values are observed during the winter when the wind speeds are higher and the air–sea temperature contrast greater; in the control run, average values of 158 W m^{-2} and 172 W m^{-2} are observed for the first and second winters, compared to 160 W m^{-2} and 173 W m^{-2} for the perturbed run. The higher heat flux during the second winter in both experiments is a response to the increased wind speed associated with the strong NAO index at this time.

[41] The 2 years of mesocyclonic forcing resulted in an additional 4.03×10^{10} J of heat being extracted from the surface of the ocean to the atmosphere, in the Nordic Seas region. A time series of the total maximum heat flux anomaly every 6 hours in the Nordic Seas highlights the additional heat flux being extracted at the model air–sea boundary, as a result of the parameterization (Figure 8b). Heat flux anomalies of over 200 W m^{-2} are repeatedly observed, with the highest heat flux anomaly of 806 W m^{-2} occurring due to the parameterization of a 323-km-diameter vortex located northeast of the Faeroe Islands (61°N, 4°E),

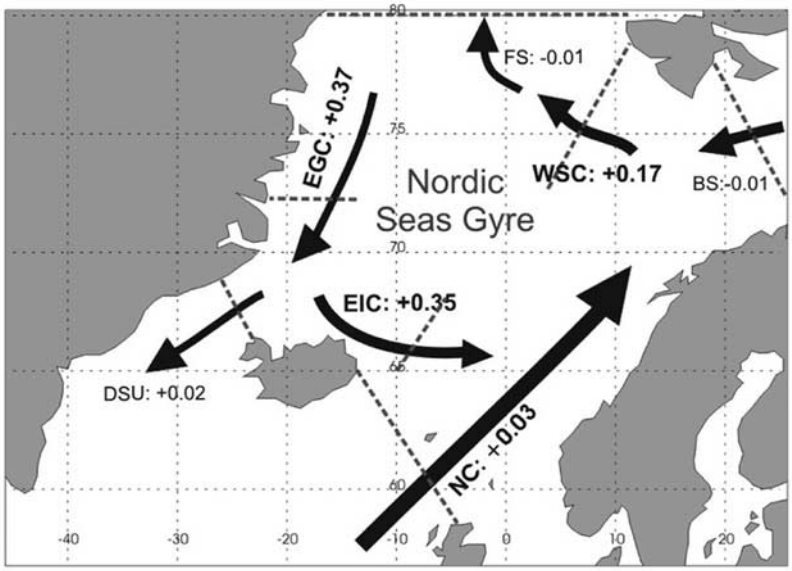

Figure 9. A schematic illustrating the spin up of the Nordic Seas gyre during the second winter (DJFM) in the perturbed run, as a result of increased volume transports in the Norwegian Current (NC), West Spitzbergen Current (WSC), East Greenland Current (EGC), and East Icelandic Current (EIC). Positive values indicate an increase in volume transport (in the direction of the arrow) in the perturbed run, compared to the control run, with the volume changes indicated in Sverdrups (Sv).

on 30 January 1994. Somewhat fortuitously, this vortex passed over Ocean Weather Station (OWS) Mike, located at 66°N, 2°E, offering us a rare chance to further validate the parameterized wind speed of this vortex. The highest wind speed observed at OWS Mike on 30 January 1994 was 26.2 m s^{-1}, which compares very well with the parameterized wind speed of 27.6 m s^{-1} for this event.

[42] Consistent with the increased heat loss from the ocean surface, the integrated heat content of the Nordic Seas had reduced by 3.6×10^{10} J at the end of the perturbed run (Figure 8c), and is in close agreement with the additional heat loss from the ocean surface during this period. The net increase in surface heat loss, and reduction in ocean heat content in the perturbed run, are due to the fact that polar mesocyclones typically occur in cold air outbreaks [*Rasmussen and Turner*, 2003], where the heat flux direction is primarily from the ocean to the atmosphere. In fact, an analysis of the direction of the latent and sensible air–sea heat fluxes in the region of each polar mesocyclone in the satellite climatology of *Harold et al.* [1999] indicates that ~90% of all vortices occurred in regions where the ERA-40 heat fluxes were upward, that is, from the ocean to the atmosphere. Thus, the enhanced wind speeds in the perturbed run will not alter the direction of the heat flux, but simply enhance the existing heat fluxes.

[43] In addition to increasing the heat flux and wind stress, *Condron* [2007] conducted several short (2–4 day) modeling studies to investigate the localized impact of three separate polar mesocyclone on ocean circulation. In each case, imposing a mesoscale cyclonic atmospheric rotation upon the ocean surface led to a divergence in the surface flow field, and a compensatory upwelling (due to Ekman pumping) at the center of each storm. The increased vertical velocities beneath each vortex of $\sim 10^{-2}$ cm s^{-1} appeared to enhance the entrainment of cooler thermocline water into the mixed layer, and cool the sea surface, although it was difficult to separate this effect from cooling associated with an enhanced surface heat loss. The observed small-scale changes in ocean circulation support the hypothesis of *Shapiro et al.* [1987] that polar mesocyclones can cause ocean stirring, while the observed upwelling of cold water is consistent with observations of the impact of hurricanes and extratropical cyclones on ocean circulation [*Price*, 1981; *Ren et al.*, 2004; *Morey et al.*, 2006].

[44] In the upper circulation of the perturbed run, the cyclonic rotation of the Nordic Sea gyre increased during the second winter (1994/1995) as a result of increased volume transports in the Norwegian, West Spitzbergen, East Greenland and East Icelandic currents, compared to the second winter in the control run (Figure 9). When averaged over this winter period, all four currents in the perturbed run show an increase in volume transport that enhances the cyclonic circulation of the gyre by 0.23 Sv, compared to the control run. The increased rotation is approximately 4 times larger than the difference in the rotation of the gyre between winter 1993/1994 and winter 1994/1995 in the control run, suggesting that the Nordic Sea gyre has been "spun-up" in response to the increased wind stress imposed upon the ocean in the perturbed integration.

[45] We find that the small winter-to-winter difference in the cyclonic rotation of the Nordic Sea gyre in the control run is a result of similar circulation dynamics during these two winters. Indeed, a recent integration of the FRUGAL model simulating the interannual variability of the Nordic Seas from 1994 to the end of 2001 [*Bigg et al.*, 2005], confirms there to be very little difference in the circulation dynamics of the Nordic Sea gyre at this time. However, if we examine the full period of integration of Bigg et al., the

winter-to-winter variability in the Nordic Sea gyre over this nearly decade long forcing period is typically between 1 and 3 Sv.

[46] We now focus our attention on the impact of the parameterization on open ocean convection by examining the difference in the production of Greenland Sea Deep Water (GSDW) in the two runs. To eliminate high-frequency noise we calculate the monthly volume of GSDW from October 1993 to September 1995, defining GSDW as a water mass with salinity between 34.88 and 34.94 and potential temperature, θ, between -0.4 to 0°C. We note that it is not possible to use the definition of GSDW given in the literature as 34.92 and $\theta \leq -1.1$°C [see *Pickard and Emery*, 1990], as the deep waters in the model differ from observations.

[47] In the control run, the volume of modeled GSDW primarily increases during the winter months in response to wintertime open ocean deep convection. If one assumes that the formation of GSDW only occurs when the modeled volume of GSDW increases, then one can calculate an average production rate of 1.00 Sv. The addition of the mesocyclone parameterization enhances the production of GSDW 60% of the time that GSDW is forming in the control run, producing an additional 1070 km^3 of GSDW; equivalent to an increase in formation rate of 0.04 Sv. We note, however, that this rate of increase is not statistically significant using a two-tailed t test at, or above, the 95% confidence interval. On occasions the rate of production of GSDW in the perturbed run was considerably higher than observed in the control run—between December 1994 and January 1995 the formation rate of GSDW increased by 20%, from 1.39 Sv in the control run to 1.67 Sv in the perturbed run.

[48] Due to our GSDW definition, our estimated rates of deep water formation cannot be directly compared with observations. We note that *Schlosser et al.* [1991] suggest a maximum GSDW formation rate of 0.47 Sv in the 1960s and 1970s, decreasing to 0.1 Sv in the 1980s, while *Rhein* [1996] showed similar results, with a formation rate of 0.42 Sv from 1982 to 1989, which reduced to 0.14 Sv from 1989 to 1993. However, the difference between the two model simulations in this study implies that the modeled changes in GSDW are a response to the perturbed atmospheric forcing, and so would be a reaction in all such models.

[49] The spin up of the Nordic Seas gyre previously mentioned has almost certainly played a central role in the increased production of GSDW in the perturbed run. The increased rotation will cause a doming of the isopycnals and bring weakly stratified waters from the interior of the Nordic Seas closer to the surface. At the same time, the increased air–sea heat loss at the surface will further weaken any vertical stratification, which together will assist in preconditioning the Nordic Seas region for deep, open-ocean convection. Concurrent with these findings, we observe a deepening of the mixed layer in the perturbed run after both winters. A maximum deepening of 357 m at 69°N, 5°W in the Norwegian Sea occurs during the second winter, and is consistent with enhanced open ocean convection at this time. The model winter mixed layer depth of 2000 m is, however, considerably deeper than the observed winter mixed layer depth of 300 m [*Nilsen and Falck*, 2006]. This likely reflects the somewhat crude nature by which the small-scale deep water convective process is dealt with in numerical models that cannot accurately resolve the spatial scale of deep convection.

[50] We investigate further the extent to which the parameterization has altered the deep circulation of the northeast Atlantic by examining the volume of intermediate and deep water overflowing the GIS ridge, via the Denmark Strait and the FSC. The volume of water overflowing into the North Atlantic at each sill reveals a large amount of short-term, high-frequency variability from October 1993 to September 1995 (Figures 10a and 10b). This variability has been observed by in situ observations [*Dickson and Brown*, 1994] and appears to be a response to the short-term, high-frequency fluctuations in wind stress imposed by the forcing [*Bigg et al.*, 2005]. In the control run, the average volume transport at Denmark Strait is -1.63 Sv (where negative values indicate a southward flow), which is in fair agreement with observational mean estimates of -2.9 and -3.4 Sv [*Dickson and Brown*, 1994; *Macrander et al.*, 2005]. The deep water volume transport (600 m to bottom) passing south through the FSC in the model had a mean flow of -1.2 Sv, and is in good agreement with observational mean estimates of -1.7 Sv [*Dickson and Brown*, 1994].

[51] The difference in the Denmark Strait overflow between the control and the perturbed runs reveals high-frequency differences that are a response to the different wind stress imposed by the mesocyclone parameterization (Figures 10c and 10d). Smoothing the data with a 30-day running mean removes much of this high-frequency variability and highlights an increase in the southward volume transport in the perturbed run, especially during the second winter. During this time, the average deep (300–600 m) overflow increased by -3.4×10^{-2} Sv (+2.4%) above the mean volume transport in the second winter of the control run. Although the increased transport of water overflowing the sill in the perturbed run appears small, it is in fact 25% of the 0.15-Sv difference in transport in this region between winter 1993/1994 and winter 1994/1995 in the control run. The small winter-to-winter variability in this overflow in the control run again highlights the somewhat similar circulation dynamics of the Nordic Sea at this time. This finding is also in agreement with modeled interannual variability observed by *Bigg et al.* [2005] and also the regional Nordic Sea model of *Köhl et al.* [2007] used to investigate changes in the Denmark Strait Overflow. However, on a longer, decadal timescale, both the Bigg et al. and Köhl et al. models show winter-to-winter variability in overflow of around 0.2–0.5 Sv.

[52] The deep water southward volume transport at the FSC shows a small, but largely persistent weakening, with average transport anomalies at the end of the perturbed run 0.01 Sv more than in October 1993 (Figure 10d). We note that during the peak in the Denmark Strait overflow of winter 1994/95, the FSC overflow had weakened by $\sim 1.4 \times 10^{-2}$ Sv; a value that is 1.2% slower than the winter overflow in the control run. Considering the total volume transport at both straits together, the parameterization lead to a total increase in southward volume transport of 6.74×10^{11} m^3 ($\sim$0.01 Sv) during the 2-year forcing period. This change in volume transport over the Greenland-Iceland-Scotland ridge is comparable to observations of the fresh-

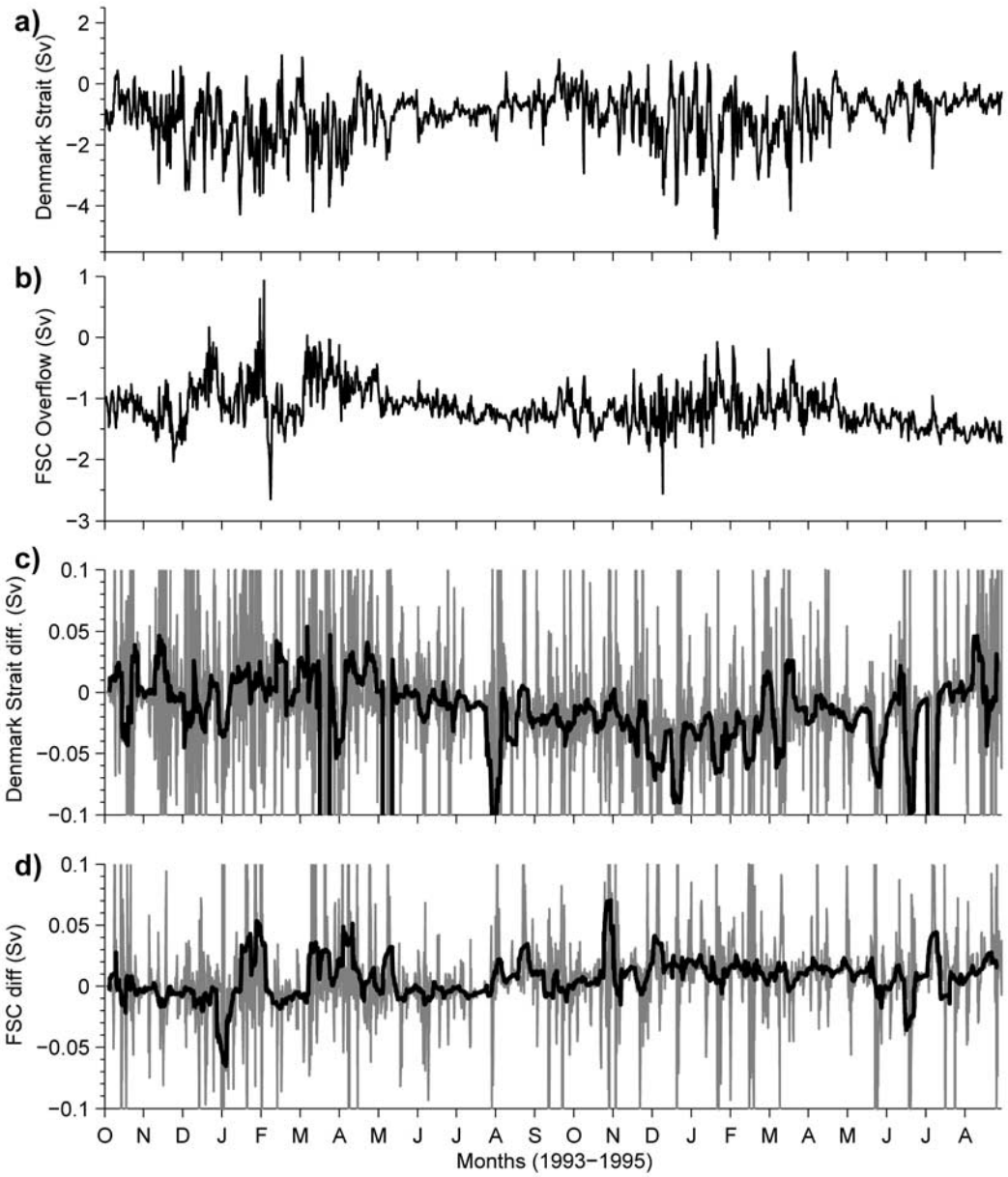

Figure 10. Volume transports (Sv) in the (a) Denmark Strait and (b) Faeroe-Shetland Channel (FSC) for the control simulation every 6 hour from October 1993 – Setepmber 1995 (southward flows are shown as negative values). (c–d) The difference in overflow between the control run and the perturbed run for the (c) Denmark Strait and (d) FSC every 6 hours (gray), and smoothed with a 30-day running mean (thick black line). An increased southward flow in the perturbed run is shown by negative values in Figures 10c and 10d.

water outflow from the Arctic to the Nordic Seas via the Barents Sea, and is approximately 15% of the 4.3×10^{12} m^3 yr^{-1} (0.1 Sv) of liquid and ice transported south at Fram Strait [*Serreze et al.*, 2006].

[53] In response to our observed increase in both deep water convection, and overflow across the GIS ridge, an increase in the strength of the Atlantic MOC might be expected. However, despite the difference in the MOC strength in the control and perturbed runs revealing a large amount of high-frequency variability, no trend in overturning was observed during this 2-year run (not shown). This was confirmed by a two-tailed *t* test that failed to show any statistically significant difference in overturning at, or above, the 95% confidence interval. It is worth noting that an increased overturning during the second winter, corresponding to the increased overflow across the GIS ridge is observed, although this increase is less than 1% above the 20.3-Sv MOC strength in the control run.

7. Summary and Conclusions

[54] The parameterization of polar mesocyclone activity over the northeast Atlantic from October 1993 to September 1995 has highlighted the importance of resolving small-

scale, high-frequency wind forcing on ocean circulation. As the resolution of ocean models improves they will become increasingly sensitive to the upper ocean wind forcing, making it vital that the fluxes at the air–sea boundary are correct. Our use of a Rankine vortex parameterization appears to be an effective template by which to include the mesocyclonic wind field of these vortices, while our size-wind speed relationship appears to do a very good job at determining the upper wind speed in all the cases we have examined.

[55] The observed spin up of the Nordic Seas gyre, increase in GSDW production, and accompanied increase in the volume transport of water across the GIS ridge highlights a clear coupling between small-scale mesocyclonic activity and changes in deep ocean circulation. The increased outflow appears to be a response to an increase in the hydraulic height of the reservoir of dense, deep water upstream of the Denmark Strait sill in the Nordic Seas, where the enhanced heat loss and wind-driven mixing due to the parameterization pushed the thermocline deeper, and increased the volume of GSDW. In the real world, the extremely large heat fluxes associated with these vortices will likely trigger localized convective overturning in regions where the stratification is weak.

[56] The modeled change in the Nordic Seas has implications for correctly determining the sensitivity and stability of the MOC, considering the pivotal role that variations in this region have been shown to play on global climate. The lack of response of the MOC to the parameterization should not necessarily be taken to indicate that mesocyclone activity does not play a role in the setting the strength of the MOC. On the contrary, we might expect a response in the strength of the MOC if the model is run for longer and the properties of the ocean have time to adjust fully to persistent mesocyclonic impact. Indeed, the subject of this longer integration of the model, with the mesocyclone parameterization implemented in the atmospheric fields, will form a forthcoming paper.

[57] Although the parameterization in this study was used to include mesoscale vortices within the ERA-40 reanalysis data, we suggest that it should be used in other atmospheric forcing data sets, and the atmospheric component of coupled atmosphere-ocean models. Ocean-only models are often forced with the NCEP reanalysis [*Kalnay et al.*, 1996], or products based on this reanalysis such as the CORE (Coordinated Ocean Research Experiments) data set [*Large and Yeager*, 2004]. However, the coarser T62 (approx. $2.5^\circ \times 2.5^\circ$) spectral model resolution, compared to the T159 resolution of ERA-40, can only begin to represent features with a size, N, above 330 km ($N = 6400\pi/62$), although for an accurate representation a value 4 times the minimum size of the grid resolution appears necessary [*Laprise*, 1992]. Therefore, the NCEP reanalysis are not likely to fully resolve vortices until they are 1300 km in size, compared to the 500-km threshold in ERA-40. Thus, ocean models forced with the NCEP reanalysis or CORE data exclude the entire range of subsynoptic-scale vortices, and their associated forcing upon the ocean, highlighting a clear requirement to include a parameterization of mesocyclone activity when using such data sets.

[58] A similar limitation arises in coupled ocean-atmosphere models, where the grid resolution of the atmosphere may be even cruder. For example, in the well established HadCM3 model used for global climate prediction, the atmosphere has an equivalent spectral resolution of T42 (3.75° longitude by 2.5° latitude). Thus, the smallest feature the atmospheric model can hope to resolve is 480 km, although if 4 grid points are required to fully resolve a feature then vortices must be ~1900 km in size. As such, coupled models would greatly benefit from our parameterization, albeit in a rather modified form, to include subgrid scale forcing in the atmospheric component of these models.

[59] Finally we note that these vortices are not only observed in the Nordic Seas, but are ubiquitous over both of the climatic important driving regions of the Labrador Sea and the Weddell Sea, Antarctica, suggesting an urgent requirement to parameterize all regions of polar mesocyclonic activity in ocean-only and coupled climate models, so as to capture the important high rates of ocean heat loss otherwise missed. It would now also timely to investigate the effect of our high-resolution atmospheric forcing on the upper ocean of a regional eddy resolving model (~0.1 degree). At this higher resolution, small-scale atmosphere-ocean dynamics would be more accurately resolved, allowing for a detailed and thorough investigation of the processes occurring in the upper ocean, and the direct mechanism by which these vortices alter deep open ocean convection, and the larger-scale circulation.

[60] **Acknowledgments.** This work was carried out under an NERC funded studentship tied to the Coupled Ocean-Atmosphere Processes and European Climate (COAPEC) thematic program and a CASE studentship award from British Antarctic Survey. We would like to thank G. Noer at the Norwegian Meteorological Institute, Tromso, Norway, for providing the list of 20 AVHRR observed polar mesocyclones used in this study.

References

Bacon, S. (1998), Decadal variability in the outflow from the Nordic seas to the deep Atlantic Ocean, *Nature*, *394*(6696), 871–874.

Batchelor, G. K. (1967), *An Introduction to Fluid Mechanics*, 635 pp., Cambridge Univ. Press, New York.

Beare, M. I. (1998), The Southampton–East Anglia (SEA) model: A general purpose parallel ocean model, *Phys. Chem. Earth*, *23*, 505–509.

Bigg, G. R., S. R. Dye, and M. R. Wadley (2005), Interannual variability in the 1990s in the northern Atlantic and Nordic Seas, *J. Atmos. Ocean Sci.*, *10*(2), 123–143.

Bryan, K. (1969), A numerical method for studying the circulation of the world ocean, *J. Comput. Phys.*, *4*(3), 347–376.

Chelton, D. B., and M. H. Freilich (2005), Scatterometer-based assessment of 10-m wind analysis from the operational ECMWF and NCEP Numerical Weather Prediction Models, *Mon. Weather Rev.*, *133*, 409–429.

Chelton, D. B., M. G. Schlax, M. H. Freilich, and R. F. Milliff (2004), Satellite measurements reveal persistent small-scale features in ocean winds, *Science*, *303*, 978–983.

Chen, D., W. T. Liu, S. E. Zebiak, M. A. Cane, Y. Kushnir, and D. Witter (1999), Sensitivity of the tropical Pacific Ocean simulation to the temporal and spatial resolution of wind forcing, *J. Geophys. Res.*, *104*(C5), 11,261–11,271.

Condron, A. (2007), The impact of polar mesocyclones on deep water formation, Ph.D. thesis, 190 pp., University of Sheffield, Sheffield.

Condron, A., G. R. Bigg, and I. A. Renfrew (2006), Polar mesoscale cyclones in the northeast Atlantic: Comparing climatologies from ERA-40 and satellite imagery, *Mon. Weather Rev.*, *134*(5), 1518–1533.

Cox, M. D. (1984), A primitive equation three-dimensional model of the ocean, in *GFDL Ocean Group Tech. Rep. 1*, p. 250, Geophysical Fluid Dynamics Laboratory/NOAA, Princeton University, Princeton.

Cunningham, S. A., et al. (2007), Temporal variability of the Atlantic meridional overturning circulation at 26.5 degrees N, *Science*, *317*(5840), 935–938.

Dickson, R. R., and J. Brown (1994), The production of North Atlantic Deep Water, *J. Geophys. Res.*, *99*(C6), 12,319–12,341.

Doscher, R., and R. Redler (1997), The relative importance of northern overflow and subpolar deep convection for the North Atlantic thermohaline circulation, *J. Phys. Oceanogr.*, *27*(9), 1894–1902.

Douglas, M. W., L. S. Fedor, and M. A. Shapiro (1991), Polar low structure over the Northern Gulf of Alaska based on research aircraft observations, *Mon. Weather Rev.*, *119*(1), 32–54.

Douglas, M. W., M. A. Shapiro, L. S. Fedor, and L. Saukkonen (1995), Research aircraft observations of a polar low at the East Greenland ice-edge, *Mon. Weather Rev.*, *123*(1), 5–15.

Eden, C., and T. Jung (2001), North Atlantic interdecadal variability: Oceanic response to the North Atlantic oscillation (1865–1997), *J. Climate*, *14*(5), 676–691.

England, M. H. (1993), Representing the global-scale water masses in ocean general circulation models, *J. Phys. Oceanogr.*, *23*, 1523–1552.

Flato, G. M., and W. D. Hibler (1992), Modeling pack ice as a cavitating fluid, *J. Phys. Oceanogr.*, *22*, 626–651.

Hakkinen, S. (1995), Simulated interannual variability of the Greenland Sea deep water formation and its connection to surface forcing, *J. Geophys. Res.*, *100*(C3), 4761–4770.

Harold, J. M., G. R. Bigg, and J. Turner (1999), Mesocyclone activity over the northeast Atlantic. part 1: Vortex distribution and variability, *Int. J. Climatol.*, *19*, 1187–1204.

Haurwitz, B. (1951), The motion of binary cyclones, *Arch. Meteorol. Geophys. Bioclimatol. B Theor. Appl. Climatol.*, *B4*, 73–86.

Hurrell, J. W. (1995), Decadal trends in the North Atlantic Oscillation: Regional temperatures and precipitation, *Science*, *269*, 676–679.

Kalnay, E., et al. (1996), The NCEP/NCAR 40-year reanalysis project, *Bull. Am. Meteorol. Soc.*, *77*(3), 437–471.

Kelly, K., and S. Dickinson (1999), NSCAT tropical wind stress maps: Implications for improving ocean modeling, *J. Geophys. Res.*, *104*(C5), 11,291–11,310.

Köhl, A., R. H. Kase, D. Stammer, and N. Serra (2007), Causes of changes in the Denmark strait overflow, *J. Phys. Oceanogr.*, *37*(6), 1678–1696.

Kurihara, Y., M. A. Bender, and R. J. Ross (1993), An initialization scheme of hurricane models by vortex specification, *Mon. Weather Rev.*, *121*(7), 2030–2045.

Laprise, R. (1992), The resolution of global spectral models, *Bull. Am. Meteorol. Soc.*, *73*, 1433–1454.

Large, Y., and S. G. Yeager (2004), Diurnal to decadal global forcing for ocean and sea-ice models: The datasets and flux climatologies, *NCAR Technical Note: NCAR/TN-460+STR*, 105 pp., CGD Division of the National Centre for Atmospheric Research, Boulder, Colorado.

Macrander, A., U. Send, H. Valdimarsson, S. Jonsson, and R. H. Kase (2005), Interannual changes in the overflow from the Nordic Seas into the Atlantic Ocean through Denmark Strait, *Geophys. Res. Lett.*, *32*, L06606, doi:10.1029/2004GL021463.

Marshall, J., and F. Schott (1999), Open ocean convection: Observations, theory and models, *Rev. Geophys.*, *37*(1), 1–64.

Morey, S. L., M. A. Bourassa, D. S. Dukhovskoy, and J. J. O'Brien (2006), Modeling studies of the upper ocean response to a tropical cyclone, *Ocean Dyn.*, *56*(5–6), 594–606.

Murray, R. J., and I. Simmonds (1991), A numerical scheme for tracking cyclone centres from digital data. part I: Development and operation of the scheme, *Aust. Meteorol. Mag.*, *39*, 155–166.

Nilsen, J. E. O., and E. Falck (2006), Variations of mixed layer properties in the Norwegian Sea for the period 1948–1999, *Prog. Oceanogr.*, *70*(1), 58–90.

Pacanowski, R. C., and G. Philander (1981), Parametrization of vertical mixing in numerical models of the tropical ocean, *J. Phys. Oceanogr.*, *11*, 1442–1451.

Parkinson, C. L., and W. M. Washington (1979), A large-scale numerical model of sea ice, *J. Geophys. Res.*, *84*(C1), 311–337.

Pickard, G. L., and W. J. Emery (1990), *Descriptive Physical Oceanography: An Introduction*, 5th ed., 320 pp., Butterworth-Heinemann, Oxford, Great Britain.

Pickart, R. S., M. A. Spall, M. H. Ribergaard, G. W. K. Moore, and R. F. Milliff (2003), Deep convection in the Irminger Sea forced by the Greenland tip jet, *Nature*, *424*, 152–156.

Pielke, R. A. (1991), A recommended specific definition of "resolution", *Bull. Am. Meteorol. Soc.*, *72*, 1914.

Price, J. F. (1981), Upper ocean response to a hurricane, *J. Phys. Oceanogr.*, *11*(2), 153–175.

Rahmstorf, S. (1995), Bifurcations of the Atlantic thermohaline circulation in response to changes in the hydrological cycle, *Nature*, *378*(6553), 145–149.

Rasmussen, E. A., T. S. Pedersen, L. T. Pedersen, and J. Turner (1992), Polar lows and Arctic instability lows in the Bear Island Region, *Tellus, Ser. A. Dyn. Meteorol. Oceanogr.*, *44A*(2), 133–154.

Rasmussen, E. A., and J. Turner (2003), *Polar Lows: Mesoscale Weather Systems in the Polar Regions*, 612 pp., Cambridge Univ. Press, New York.

Ren, X. J., W. Perrie, Z. X. Long, and J. Gyakum (2004), Atmosphere-ocean coupled dynamics of cyclones in the midlatitudes, *Mon. Weather Rev.*, *132*(10), 2432–2451.

Renfrew, I. A., G. W. K. Moore, and A. A. Clerk (1997), Binary interactions between polar lows, *Tellus, Ser. A. Dyn. Meteorol. Oceanogr.*, *49*(5), 577–594.

Rhein, M. (1996), Convection in the Greenland Sea, 1982–1993, *J. Geophys. Res.*, *101*(C8), 18,183–18,192.

Schlosser, P., G. Bonisch, M. Rhein, and R. Bayer (1991), Reduction of deep-water formation in the Greenland Sea during the 1980s—evidence from tracer data, *Science*, *251*(4997), 1054–1056.

Semtner, A. J. (1974), An oceanic general circulation model with bottom topography, *Tech. Rep. 9*, 99 pp., UCLA, Department of Meteorology, Los Angeles, California.

Serreze, M. C., A. P. Barret, A. G. Slater, R. A. Woodgate, K. Aagaard, R. B. Lammers, M. Steele, R. Moritz, M. Meredith, and C. M. Lee (2006), The large-scale freshwater cycle of the Arctic, *J. Geophys. Res.*, *111*, C11010, doi:10.1029/2005JC003424.

Shapiro, M. A., L. S. Fedor, and T. Hampel (1987), Researchg aircraft measurements of a polar low over the Norwegian Sea, *Tellus*, *37A*, 272–306.

Shaw, G., and D. Wheeler (2000), *Statistical Techniques in Geographical Analysis*, 359 pp., David Fulton Publishers, London, Great Britain.

Simmons, A. J., and J. K. Gibson (2000), The ERA-40 Project Plan. (Available at http://www.ecmwf.int/publications/library/ecpublications/_pdf/era40/ERA40_PRS_1.pdf)

Singh, R., P. K. Pal, C. M. Kishtawal, and P. C. Joshi (2005), Impact of bogus vortex for track and intensity prediction of tropical cyclone, *J. Earth Syst. Sci.*, *114*(4), 427–436.

Wadley, M. R., and G. R. Bigg (2002), Impact of flow through the Canadian Archipelago and Bering Strait on the north Atlantic and Arctic circulation: An ocean modelling study, *Q. J. R. Meteorol. Soc.*, *128*(585), 2187–2203.

Wunsch, C. (2005), The total meridional heat flux and its oceanic and atmospheric partition, *J. Climate*, *18*(21), 4374–4380.

G. R. Bigg, Department of Geography, University of Sheffield, Winter Street, Sheffield, S10 2TN, UK.

A. Condron, Department of Earth, Atmospheric and Planetary Sciences, Massachusetts Institute of Technology, 77 Massachusetts Avenue, Cambridge, MA 02139, USA. (acondron@whoi.edu)

I. A. Renfrew, School of Environmental Sciences, University of East Anglia, Norwich, NR4 7TJ, UK.